

Terahertz-driven acceleration of subrelativistic electron beams using tapered rectangular dielectric-lined waveguides

Laurence J. R. Nix^{1,2,*} Joseph T. Bradbury^{1,3} Christopher T. Shaw^{1,3}
 Morgan T. Hibberd^{1,3} Darren M. Graham^{1,3} Robert B. Appleby^{1,3}
 Graeme Burt^{1,2} Rosa Letizia^{1,2} and Steven P. Jamison^{1,4}

¹*The Cockcroft Institute, Sci-Tech Daresbury, Keckwick Lane, Daresbury, Warrington WA4 4AD, United Kingdom*

²*School of Engineering, Lancaster University, Bailrigg, Lancaster, LA1 4YW, United Kingdom*

³*Department of Physics and Astronomy & Photon Science Institute, The University of Manchester, Oxford Road, Manchester M13 9PL, United Kingdom*

⁴*Department of Physics, Lancaster University, Bailrigg, Lancaster, LA1 4YW, United Kingdom*

 (Received 22 December 2023; accepted 25 March 2024; published 11 April 2024)

We investigate the use of tapered rectangular dielectric-lined waveguides (DLWs) for the acceleration of low-energy, subrelativistic, electron bunches by the interaction with multicycle narrowband terahertz (THz) pulses. A key challenge exists in this subrelativistic regime; the electron velocity changes significantly as energy is gained. To keep electrons in the accelerating phase, the phase velocity must also be increased to match. We present simulations which demonstrate that the dielectric thickness can be kept constant and the width of the dielectric lining can be tapered along the direction of travel to vary the phase velocity, an approach only possible by the use of a rectangular waveguide geometry. The properties of tapered DLWs are discussed and following this, a design process is presented to demonstrate that the way this tapering can be optimized for different pulse and beam parameters. The minimum accelerating gradient for electron bunch capture is derived and compared to simulations. As examples of this design process, designs are considered based on considerations of the THz source, incoming electron beam, and manufacturing tolerances. A maximum THz pulse energy of 22.5 μJ in the DLW was considered, which represents what is readily achievable using mJ-level regenerative amplifier laser systems together with optical-to-terahertz conversion in lithium niobate crystals. This will be more than double the energy of a 100 keV electron beam, increasing it to 205 keV. We describe the optimization process and present a detailed exploration of the beam dynamics, discussing how the performance will further improve with compressed bunches.

DOI: [10.1103/PhysRevAccelBeams.27.041302](https://doi.org/10.1103/PhysRevAccelBeams.27.041302)

I. INTRODUCTION

Terahertz (THz) waveguides have received interest in recent years and are commonly used as a confined, low loss way to transport THz waves. They are now beginning to show great promise in a variety of applications, driven by the high demand in areas, such as 6G telecommunications and signal processing [1–5], submillimeter biological and chemical sensors [6–9], as well as terahertz imaging, microscopy, and spectroscopy [10–13]. With the recent advent of THz sources with peak electric fields exceeding the GV m^{-1} level [14], terahertz waveguides have found another highly effective application; as a structure for

mediating THz-electron beam interactions. One common approach to this technique is to use a dielectric-lined waveguide (DLW) to match the phase velocity to the beam velocity while also controlling THz pulse dispersion. Such devices have been studied and used in demonstrations of electron acceleration [15–23], deflection/streaking [16,24–27], bunch compression [17,28–30], energy modulation [18,31–34], and jitter suppression [22,28].

The mm-scale wavelengths in the THz regime offer excellent control over the phase space of picosecond electron bunches, with pC-level charge [16,18], while not being so short as to introduce significant challenges from manufacturing tolerances imposed by the use of optical frequencies, as is the case with dielectric laser accelerators (DLAs) [35–37]. The submicronwide channels of DLAs, which are set by the optical driving wavelength, also make bunch injection challenging, although there have been recent demonstrations of energy gains from 28 to 41 keV [36] and 96 to 120 keV [37]. Terahertz radiation therefore exists in an ideal region to be readily exploited by

*l.nix@lancaster.ac.uk

Published by the American Physical Society under the terms of the *Creative Commons Attribution 4.0 International* license. Further distribution of this work must maintain attribution to the author(s) and the published article's title, journal citation, and DOI.

emerging THz generation techniques for building compact accelerators with precise control over picosecond bunches.

Demonstrations of THz-driven acceleration in DLWs have utilized a traveling THz wave, whose accelerating phase co-propagates with an electron bunch [15,19]. Narrowband terahertz pulses have been used to demonstrate a prolonged interaction [18], which is often limited in these devices by pulse walk off caused by low group velocity, and phase slippage caused by a difference in the phase velocity compared to the beam velocity. In relativistic cases, the phase-velocity-matching issue is mitigated by the approximate constancy of particle velocity with energy growth. This means a straight DLW of constant cross section is capable of matching the THz phase velocity v_p with the electron velocity $v_e \approx c$ along its length. The THz-driven acceleration of subrelativistic beams in DLWs remains challenging, however, as accelerated particles are prone to overtake the accelerating phase of the driving radiation in straight waveguides. Various methods have been suggested to combat this phase slippage, including the use of vacuum channel phase shifters with constant dielectric thickness and varying metal channel width [38] and waveguides with a dielectric lining of tapered thickness [39]. Each of these methods aims to modify the THz phase velocity along the longitudinal direction of the waveguide and ensure that accelerating THz phase remains synchronous with the particle beam.

Tapered DLWs offer a promising way to maintain synchronism with a subrelativistic accelerating beam, having been proposed for use in both THz-driven and laser-driven schemes [39,40]. It has been shown that structures of this type can offer stable synchronism with minimal change to the particle acceleration over a variety of input powers [39]. To achieve any substantial acceleration, electrons and the THz pulse must travel through the structure together with velocities matched such that the electrons remain in an accelerating phase across the interaction length. To match the phase velocity v_p to a subrelativistic electron velocity $v_e < c$, a structure that can support subluminal phase velocities is required. The rectangular dielectric-lined waveguide [27,31,41] is well suited for this purpose, with the minimum available phase velocity determined by the thickness of the dielectric layer and the dielectric constant of the material. Using dielectric linings on the order of a couple of hundred microns thick, it is possible to fine-tune the accelerating mode phase velocity, v_p to well below c , and therefore it is possible to synchronize with a subrelativistic electron beam. Some existing studies have been based on cylindrical DLWs with tapered dielectric thickness [39]. Here, we instead look to rectangular structures that allow a new approach whereby the dielectric thickness can be kept constant and the width of the dielectric lining can be tapered to vary the phase velocity. This is advantageous from a manufacturing perspective as it allows the tapered shape to be cut from a ready-made sheet of the chosen material. The rectangular shape also enables the

possibility of sliding parts that can tune the synchronous frequency range as well as flexibility over the method of coupling THz radiation into the structure.

In this work, we present the design process for the production of a tapered DLW. We show how the consideration of manufacturing limitations can lead to a design which is achievable in a workshop. We then demonstrate how a close connection between the design choices and the transverse and longitudinal beam dynamics can yield an optimized structure with enhanced beam preservation properties. We then show how we have used this process to design a tapered DLW. A specific case is considered where the aim is to accelerate 100 keV bunches from a commercially available dc photoelectron gun [42] using 0.2 THz multicycle pulses generated using the output from a commercial regenerative Ti-Sapphire amplifier system [43]. This gun is selected as it is a common off-the-shelf model, but the design principles we discuss would remain relevant with starting energies up to several hundred keV.

The layout of this paper is as follows: In Secs. II A and II B, we introduce the general design principles and electromagnetic properties of tapered DLWs. In Sec. II C, we describe how the frequency choice influences the structure design, and in Sec. II D, we explain the optimization process for a tapered DLW designed to accelerate subrelativistic electrons. In Sec. III, we report on the complete transverse and longitudinal beam dynamics for a tapered DLW designed using our methodology, detailing the modeling process in Sec. III A, and the beam dynamics results in Sec. III B. Here we show how detailed consideration of the simulated beam dynamics can influence the design choices. Finally, in Sec. IV, we explore how solving the challenging problem of maintaining synchronicity with a subrelativistic beam can open the door to a scaled up THz beamline, constituting successive tapered DLWs designed using our scheme. We explain how such a linac would be capable of producing high-quality, high-energy beams, with low transverse emittance and energy spread.

II. GENERAL PROPERTIES AND DESIGN OF TAPERED DLWs

In this section, the properties of rectangular DLWs are discussed. We use a thick layer of fused silica in order to match the low beam velocity; however, this results in a mode that is mostly trapped within the dielectrics reducing the impedance. The implications of this for THz applications are discussed with trade-offs, showing how it makes for a suitable electron acceleration structure. We present the principles of tapered DLWs and how practical considerations for manufacture can guide design choices when developing structures of this type.

A. General DLW design principles

In Fig. 1, we define the geometric variables in the dielectric-lined waveguide (DLW) and illustrate an

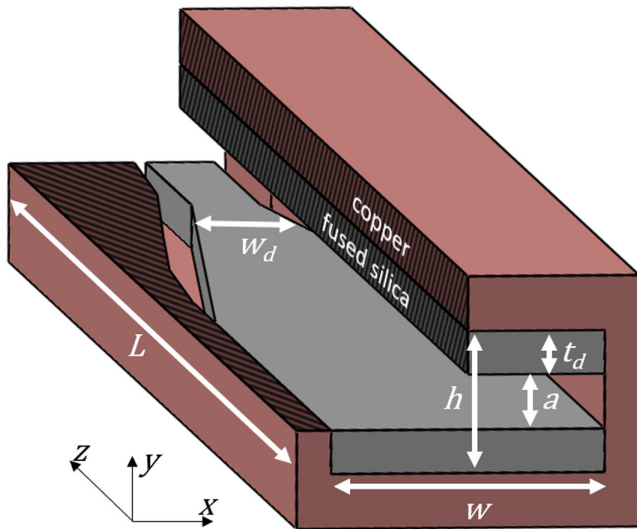


FIG. 1. Cutaway view of a width-tapered rectangular DLW with metal width w , dielectric width w_d , vacuum gap height a , dielectric thickness t_d , full height h , and length L . The direction of propagation is the z direction with the axis defined as the center line of the waveguide.

example tapering scheme. The accelerating mode in a rectangular DLW of this type is the longitudinal section magnetic mode, LSM_{11} [31,41], which has a strong longitudinal electric field component on axis. The x and y components are zero on axis, but off-center particles will experience transverse forces as discussed further in Sec. III. The properties of this mode can be controlled by careful assignment of the variables in Fig. 1. To taper this structure, the manufacturing practicalities must be considered. First, t_d should be constant as machining a varying thickness on a fused silica sheet is not feasible to the precision needed. Second, in this case with a thick dielectric layer, varying h (and hence a) has little to no impact on the group and phase velocities. The gap height a should be chosen to allow sufficient clearance between the beam edge and dielectric surface. While using the smallest a possible raises the field-on-axis, it can also increase the curvature of the field across beam radius and increase the deflecting fields for off axis particles. For our design, we have selected $a = 0.48$ mm based on the simulated beam dynamics of a commercially available dc electron gun. The FWHM beam radius upon entry is around $80 \mu\text{m}$, and we allow triple this value either side of the axis. This leaves only the widths w and w_d as available parameters for the tapering.

The eigenmode solver in CST Studio Suite [44] was used to calculate waveguide properties. By use of a periodic boundary condition in the direction of propagation and a fixed phase advance across that boundary, the phase velocity of a given mode and frequency can be found. Repeating this calculation for cross sections of different widths, it is simple to construct a picture of how v_p varies as the structure is tapered.

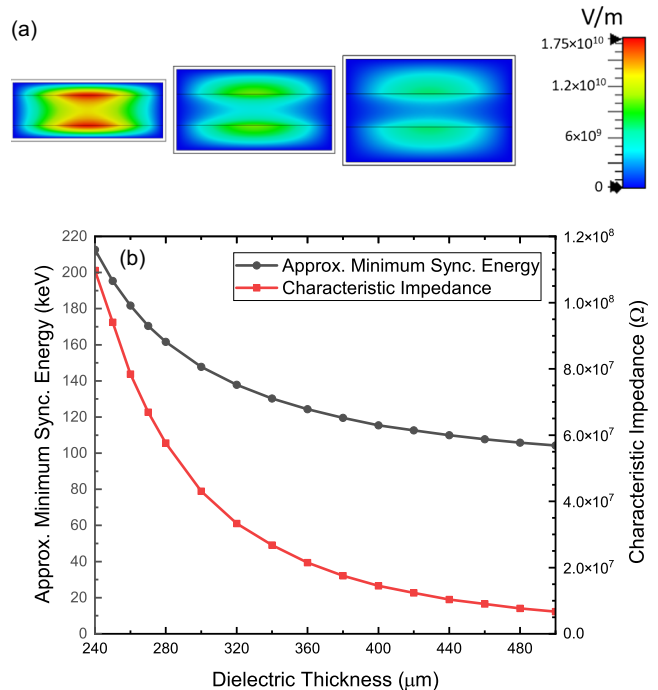


FIG. 2. Illustration of field trapping in DLWs. (a) The maximum longitudinal electric field (for arbitrary total mode energy) in DLWs with the same gap height and increasing dielectric thickness. (b) Characteristic impedance and minimum synchronous energy for 0.2 THz DLWs with increasing thickness of dielectric layer and constant a and w .

B. Properties of tapered waveguides

This section describes the effect of width tapering in a rectangular DLW. For consistency with later sections, this analysis is presented at a frequency of 0.2 THz, but trends and principles discussed remain applicable at other operating frequencies. Likewise, for consistency, we show structures with our chosen gap height $a = 0.48$ mm. For structures with dielectric linings as thick as ours, the sensitivity of group and phase velocity to gap height is extremely low. When particle energies and the phase experienced by particles are discussed in this section, we refer to a single reference electron, neglecting the nonzero duration and transverse size of the bunch until Sec. IID where a realistic bunch is considered.

Figure 2 illustrates the maximum accelerating field for a 0.2 THz signal in example DLWs with different dielectric thicknesses. When the dielectric layer is thick, the field is mostly trapped, thus leaving low field on axis. However, the minimum available synchronous velocity in a structure depends on the dielectric thickness. Therefore, to reach a lower minimum synchronous velocity, it is necessary to also lower the accelerating gradient.

Figure 3(a) illustrates the widths at which $v_p = v_e$ for a 0.2 THz pulse propagating in a fused silica DLW with $a = 0.48$ mm and $t_d = 0.38$ mm. Using a different value of t_d or relative permittivity ϵ_r shifts the position of the curve,

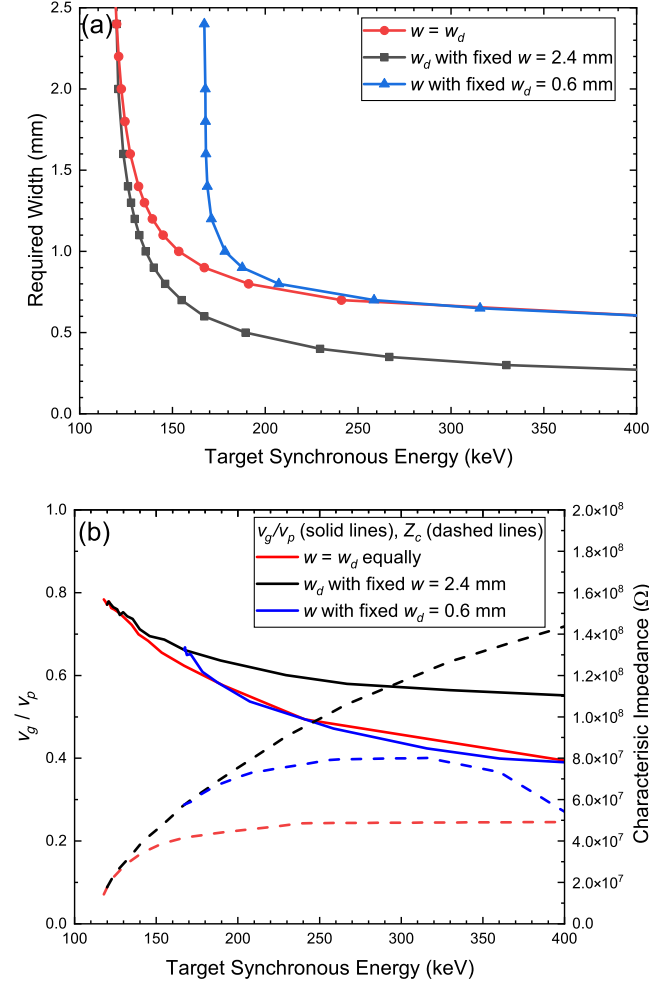


FIG. 3. (a) Widths required to synchronize the phase velocity of a 0.2 THz pulse and an electron of a given energy in a fused silica DLW with $a = 0.48$ mm and $t_d = 0.38$ mm. (b) Group velocity and characteristic impedance on axis (for arbitrary total mode energy) in waveguide sections synchronized to electron energy.

but the general shape remains similar. The dielectric material and thickness here were chosen to match the readily purchasable wafers that gave the most suitable range of available synchronous velocities at 0.2 THz. Silica was selected for manufacturing reasons, though in principle one may design a dielectric-lined structure using a different material, such as silicon [45], and alternative materials may remain of interest for future design studies.

The near-vertical region of Fig. 3(a) effectively sets a minimum electron energy for which synchronism can be achieved. Use of a thicker dielectric would lower this minimum value but would also lower the field on axis as shown in Fig. 2. This means that synchronization from 100 keV would be possible with a thicker dielectric, but the accelerating gradient would be lower. However, it is not necessary or optimal to synchronize perfectly from the injection energy. If a particle is injected off-crest but within the accelerating bucket, it will still gain energy and will

have improved bunching due to the time variation of the electric field providing more acceleration to the tail of the bunch than the head. If this nonsynchronous off-crest acceleration raises a particle above the minimum synchronous energy before it drifts into a decelerating phase, that particle can be captured for acceleration along the full structure length. In addition, the bunch can be compressed to a smaller bunch length as it accelerates toward synchronism. This velocity mismatch issue is similar to that considered in [46,47], where an equation is derived to calculate the minimum required electric field for a low-energy beam in a $v_p = c$ linac. Modifying the derivation to accommodate a subluminal phase velocity $\beta_p = v_p/c$, we can arrive at an equation for the phase slippage

$$\sin \phi = \sin \phi_i + \frac{2\pi mc^2}{qE_0\lambda} \left[\frac{\frac{1}{\beta_p} - \beta_i}{\sqrt{1 - \beta_i^2}} - \frac{\frac{1}{\beta_p} - \beta}{\sqrt{1 - \beta^2}} \right], \quad (1)$$

where β_i is the initial electron velocity (normalized to c), β_p is the chosen minimum phase velocity of the structure, ϕ_i is the injection phase, and E_0 is the longitudinal electric field strength. For capture to be possible, the electron velocity must rise from β_i to β_p before the electron slips out of the accelerating bucket. Therefore, the maximum allowable slippage is from -90° to $+90^\circ$. Upon inserting these values, Eq. (1) may be rearranged to define the electric field condition required for capture, giving

$$E_0 > \frac{\pi mc^2}{q\lambda} \left[\frac{\frac{1}{\beta_p} - \beta_i}{\sqrt{1 - \beta_i^2}} - \frac{\frac{1}{\beta_p} - \beta_p}{\sqrt{1 - \beta_p^2}} \right]. \quad (2)$$

Equation (2) provides an absolute minimum wherein the phase slippage moves the reference particle to the tail end of the accelerating bucket. An idealized design would see no overshoot, but in Sec. IID, we shall discuss that the unavoidable overshoot when working with fields below $2E_0$ can actually be beneficial in a practical design. Larger phase overshoot behind crest means more time with particles experiencing less acceleration, so it appears attractive to work with the highest available field. However, working with a higher accelerating field also entails higher transverse fields for off-axis particles and can therefore lead to larger transverse spreading and increased deposition rate to the structure walls. On the other hand, a higher gradient design would require less phase overshoot and therefore allow particles to spend more time close to crest where transverse forces are weak, though the beam size means that they are never zero at all relevant points. These opposite effects make it complicated to predict the relative transverse characteristics of different designs without a complete design study. Transverse issues may also be alleviated with the addition of a focusing magnet at the structure entrance to keep all particles close to on axis. For a fixed maximum pulse

energy, having that energy delivered at a modest amplitude over more THz cycles may offer better transverse performance and more room for control over bunch characteristics than if the same energy was delivered over a smaller number of cycles with higher amplitude, though in principle, the design process can be carried out for any pulse that satisfies Eq. (2). Additionally, perfect velocity matching along the full length would require mechanically unfeasible tapering, and an accelerating field that does not vary with transverse position, so there may be a region where $v_e > v_p$ and hence phase slippage in the opposite direction will occur. In that case, a small amount of phase overshoot is beneficial so that the forward slippage is toward crest. In addition, the transverse fields are defocusing on one side of the crest while focusing on the other, depending on if the offset is in the vertical or horizontal plane [21]. These transverse fields are zero on crest, so the overshoot will cause focusing transverse effects, which can be advantageous, depending on the size of the overshoot. These assertions are applicable to both rectangular and cylindrical tapered DLWs.

A further constraint on the accelerating field arises from the available THz pulse energy and duration. Since $v_g < v_p$ in the DLW, a long pulse duration is desirable to extend the walk-off length, and a high-amplitude field is desirable to increase the accelerating gradient. Laser generation of multiple-cycle THz pulses using periodically poled lithium niobate (PPLN) wafer stacks allows control over the pulse duration and amplitude [48], allowing for flexibility in the choice of pulse parameters used in optimization.

In Fig. 3(b), it is clear that tapering only the dielectric would be preferred, as this would maximize both the accelerating gradient and the group velocity. However, from a manufacturing perspective, the easiest option would taper only the metal, but this only offers significant control over phase velocity when the metal width is slightly larger than the dielectric width. Since the relationship between synchronous velocity and width is nonlinear, a taper featuring a complex curve or some approximation to it using several linear slopes seems desirable. Unfortunately, cutting the fused silica sheet into a complex shape is not practical. The shape in the dielectric layer is to be machined with a straight-edged saw and hence straight edges in the dielectric taper are preferred. In this study, we choose to limit our silica geometry to a length of constant width, followed by a linear taper down to some minimum width, then another length of constant width. Additional control may be achieved by tapering the metal, which can be manufactured to much higher precision and need not be limited to simple tapers. The combinations of w and w_d shown in Fig. 3 are examples only; any combination may be used and they may be simultaneously tapered at different rates. For this paper, we taper both w and w_d at different rates to achieve the most precise level of control that is practically achievable with current methods. A design in which only the dielectric is tapered would likely be better in simulation but suffers larger manufacturing defects if built.

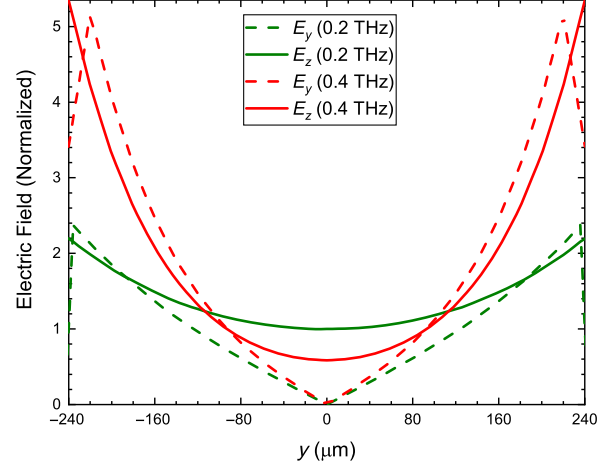


FIG. 4. Field profiles along vertical axis of the vacuum gap in example 0.2 THz and 0.4 THz DLWs. Both examples used a gap height of 0.48 mm and are normalized to set the 0.2 THz amplitude on axis to 1.

C. Frequency choice

For our work, there are a range of possible frequencies that can be used. The conversion efficiency of THz sources is relatively independent of the THz frequency range considered in this work, at around 0.14% [48]. Hence the THz pulse energy available is determined by the laser energy. Here we make a comparison between frequency choices of 0.2 and 0.4 THz, where the possible pulse energies are approximately identical. The normalized electric field strength across the vertical axis is shown in Fig. 4 for two DLWs with these operating frequencies, each with $a = 0.48$ mm.

Multiple advantages of selecting 0.2 THz are apparent. Although the maximum value of E_z is much higher in the 0.4 THz case, it is the field at the center that is most relevant. The beam radius is around 80 μm , and within this range, the 0.2 THz option has a higher and more uniform value of E_z . For the 0.2 THz waveguide option, the initial electron velocity was $0.548c$, and the initial phase velocity was $0.587c$. Inserting these values into Eq. (2), we obtain the requirement that the accelerating field required for capture $E_0 > 2.45$ MV/m. The 0.4 THz alternative achieved a slightly lower initial phase velocity of $0.576c$, but since Eq. (2) is also inversely dependent on wavelength, the benefit of the smaller velocity difference is cancelled and we obtain the requirement that $E_0 > 2.55$ MV/m. A 40 ps pulse would need to carry approximately 50 μJ of energy to meet the minimum field requirement in the 0.4 THz DLW but just under 10 μJ in the 0.2 THz DLW.

Each structure has a range of injection phases that can be captured. Electrons outside of the capture phases experience a variation in accelerating and decelerating fields and hence are not synchronous with the THz field. Lower frequencies enable larger duration electron bunches to be captured. In a THz accelerator constituting multiple structures, it may be beneficial to start with a lower frequency

for the first few stages in an injector and increase the frequency for later structures as the bunch length reduces due to compression by the THz fields. In the highly relativistic regime, a much thinner dielectric layer may be used thus giving on-axis accelerating field. As a consequence of the Panofsky-Wenzel theorem [49], the smaller variation in E_z field transversely means that the deflecting E_y field is lower at all points, also providing an improved beam quality and lower charge losses. Additionally, the physical scale of components at 0.2 THz compared with 0.4 THz reduces the manufacturing challenge slightly and alleviates the problem of ohmic losses due to surface roughness. Lower frequencies, below 0.2 THz, were not considered due to the lack of high field, short pulse sources.

As a result of the factors discussed here, we have chosen 0.2 THz as the frequency we use for the design of a tapered DLW in our specific example.

D. Optimization of the 0.2 THz design

Two designs for a 0.2 THz accelerating structure have been considered. The first design was based on a 22.5 μJ THz pulse, and the second design was based on a 12 μJ pulse (referring to energy inside the DLW). These values were selected based on the expected performance of using a 13 mJ commercial regenerative amplifier laser system together with periodically poled lithium niobate wafer stacks to generate multicycle THz pulses [48]. Simulation results using CST informed a conservative estimate of 60% coupling efficiency between the source and the DLW accelerating mode. When the 22.5 μJ pulse was delivered over 10 cycles (50 ps), the electric field was sufficient to satisfy Eq. (2) and hence overcome the velocity mismatch. A 12 μJ pulse delivered over 8 cycles (40 ps) was also found to be suitable, with an on-axis field of around 2.8 MV/m. Figure 5 illustrates the result of Eq. (1) for the minimum field and the approximate

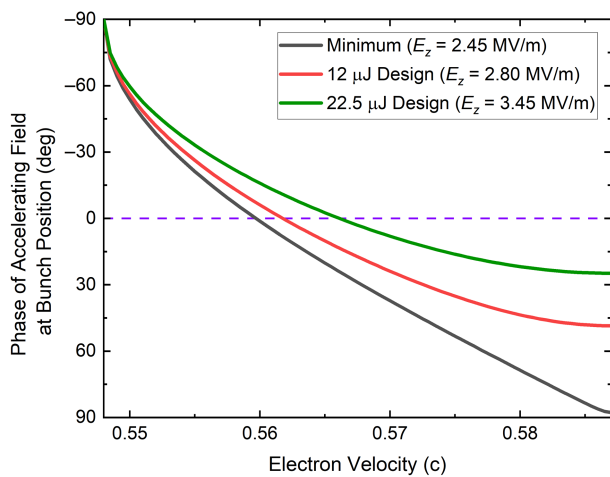


FIG. 5. Modeled phase of the accelerating field at the position of a reference electron during the mismatched section in our two designs.

field of our two design options. This serves as a rough indicator for the phase overshoot, not accounting for pulse rise time, pulse flatness, or the option of beginning the taper early. A perfectly velocity-matched design would see the particles reach crest and match the minimum phase velocity at the same point, from which tapering could begin. This section discusses why perfect velocity matching is not realistic in practice and shows that some levels of overshoot can be beneficial.

The initial waveguide geometry was estimated based on the trends illustrated in Fig. 3. CST Studio Suite [44] was then used to perform parameter sweeps over several width markers along the length. This initial stage of optimization was performed using a point source for electrons and an arbitrarily long THz pulse to ensure full-length interaction. With an approximate structure established, all further optimization of the design was performed with a beam imported from GPT simulations (Sec. IV) developed to accurately represent a commercial 100 keV electron gun. The geometry shown in Fig. 6 was calculated as an effective design for this combination of THz source and electron gun.

To compare the different structures during the parameter sweeps, the energy gain, energy spread, and capture rate were considered, where the capture rate was defined as the proportion of injected particles which exit the waveguide having synchronously accelerated to a high energy. A total waveguide length of 25 mm was selected as this was where accelerating gradient tailed off to negligible levels due to pulse walk off in an 8-cycle pulse with an initial group velocity of $0.45c$. The resulting energy growth of the captured bunch along the propagation axis is shown in Fig. 7, which illustrates an initially low gradient in the off-crest region, followed by a high rate of acceleration between 15 and 20 mm before pulse walk off at the waveguide end. In this paper, the captured bunch is defined as the particles within twice the FWHM of the peak in a histogram of the final energy distribution. The total energy gain was 62 keV over 25 mm using a 12.5 μJ THz pulse, while the design optimized for a 22.5 μJ pulse displayed a simulated energy gain of 105 keV.

Figure 8 illustrates v_e , v_p , and v_g along the length in each of the two designs and Fig. 9 shows the phase of the electric field at the center of the bunch as a function of longitudinal

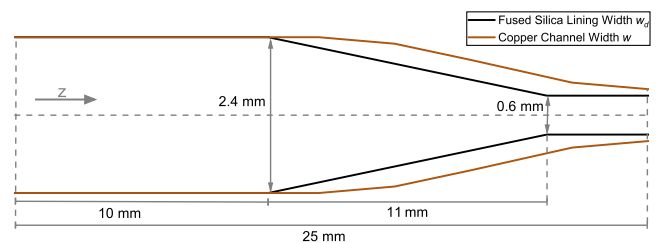


FIG. 6. Widths of the dielectric lining and metal channel along the length of the structure. The gap height (0.48 mm) and dielectric thickness (0.38 mm) are constant.

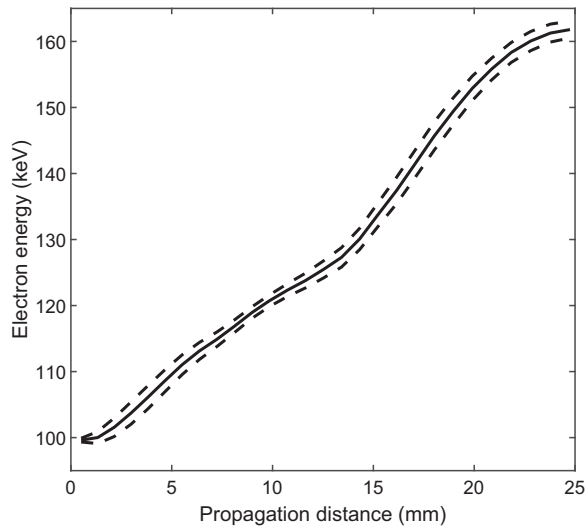


FIG. 7. Energy growth for the captured bunch in a 0.3 fC bunch from a commercially available electron gun [42] during propagation through the DLW. The solid line shows the mean energy of the captured bunch, and the dashed lines indicate the energy spread of the captured bunch.

position. The particle data shown in Fig. 8 show the full bunch sampled at 5 ps intervals with each dot representing a single electron. Due to the velocity mismatch, our modeling shows that particles overshoot the crest as in Fig. 5, which is consistent with the results in Fig. 9(b). Once the mismatch has been overcome, the phase velocity is increased by tapering. However, due to the aforementioned manufacturing constraints and the nonlinear trend in Fig. 3(a), it is not possible to perfectly match the phase throughout. Since a large change in width is required for a small change in synchronous velocity at the low-energy end of Fig. 3(a) while at the high end the opposite is true, our restriction to a linear dielectric taper means that tapering steeply enough for exact matching at the beginning would mean tapering too steeply later. Fortunately, it is actually beneficial to allow $v_p < v_e$ here because this allows forward slippage to counter the overshoot. When the overshoot particles have been realigned back to the crest, we can then aim to keep the head of bunch slightly ahead of crest such that the lower energy particles at the tail receive the most acceleration to improve capture and flatten the energy profile. In the final few mm of our design, the pulse walk-off effect meant the bunch experienced a lower accelerating field so optimization of the tapering in this region offered only minor benefit. Using a narrower width than that which would neatly match v_e and v_p provided around 1% improvement to energy and a similarly small improvement to the energy spread. This is because a narrower DLW has a higher accelerating field on axis. It also has a higher phase velocity that shifts the bunch forward in phase meaning the peak field is experienced by the lower energy back of the bunch, thus flattening its

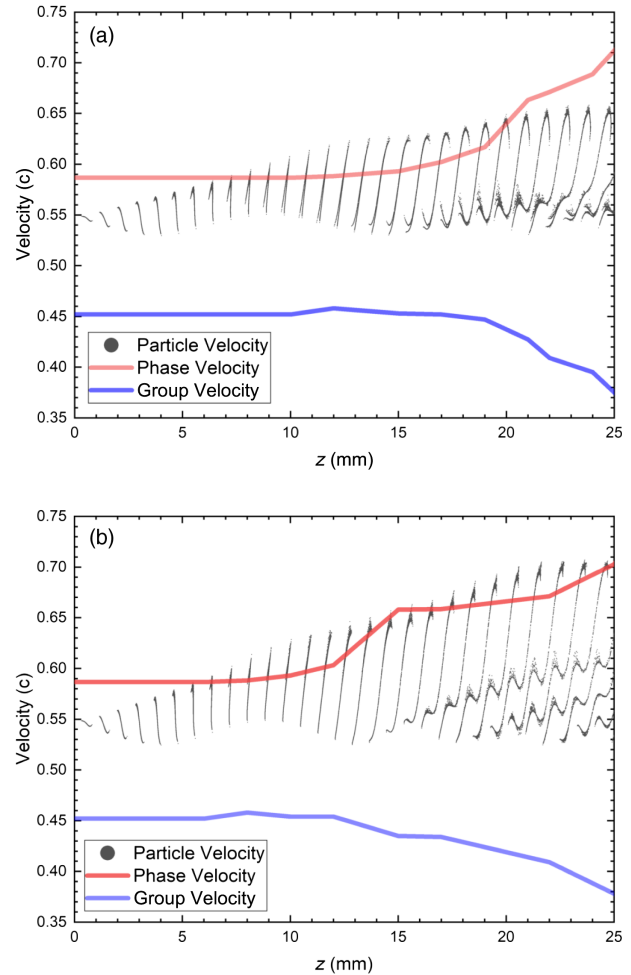


FIG. 8. Velocity of particles and waves along the structure length for (a) the 12 μJ design and (b) the 22.5 μJ design. The particle data show the full bunch at 5 ps snapshots with each dot representing a single electron.

energy profile. In the 22.5 μJ design, less phase overshoot was necessary. This allowed for more of the interaction length to use a close-to-crest phase alignment, while the lower energy design must spend a significant portion of the interaction length to slip back to the ideal phase alignment.

In this section, we have discussed the key design choices required in developing a THz-driven tapered DLW and explained the process for optimizing parameters of the design, such as the frequency choice, structure geometry, and tapering profile. We simulated the effective acceleration and capture of an electron bunch in a tapered DLW and demonstrated the bunch-phase alignment required to do so. We have compared the general performance of designs driven by low and modest pulse energies, demonstrating that significant acceleration can still be achieved in the lower energy case. In the following section, the beam dynamics considerations of the interaction are discussed in detail, focusing on the lower energy design. We assess the energy spread and transverse emittance, as well as

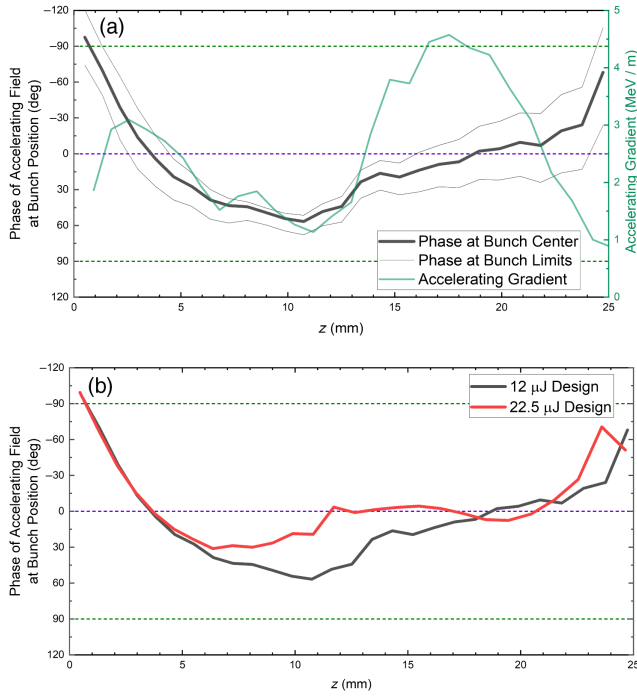


FIG. 9. Electric field phase experience by the bunch for a realistic bunch tracked from the gun using GPT and injected into the structure. (a) shows the phase of the electron bunch throughout interaction in the $12 \mu\text{J}$ design along with the corresponding field. In (b), this is compared with the higher energy design, which requires less phase overshoot.

discussing the overall performance using electron bunches injected after varying degrees of compression. This allows us to assess the ultimate performance of our tapered DLW design when used in a range of applications.

III. ELECTRON BEAM DYNAMICS

In this section, we consider the modeling of the electron beam, its interaction with the field in the structure and the evolution of key electron bunch parameters. This process allows a complete evaluation of the performance of the structure designed in this paper and demonstrates that the considered structures maintain the incoming beam quality under acceleration. We consider the acceleration and evolution of 100 keV electron bunches through the $12 \mu\text{J}$ structure.

To assess the performance and beam quality, both the longitudinal and transverse dynamics of the THz-electron beam interaction need to be analyzed in detail. For this, the results are obtained using two computational tools. The first is particle-in-cell (PIC) modeling using CST Studio Suite [44], which recorded the coordinates of electrons in the bunch in six-dimensional phase space during their propagation through the structure. The particle data were recorded in snapshots at intervals of 5 ps . The second tool is general particle tracer (GPT) [50], which tracks electrons

in the presence of applied electromagnetic fields and space-charge forces.

In this section, we review the tools and models used and then assess the performance and the beam quality preservation properties of the $12 \mu\text{J}$ structure presented in Sec. II D. Alongside simulating the tapered DLW performance with realistic GPT-generated bunches from an electron gun, we also show results from PIC simulations beginning with shorter duration, hypothetically compressed bunches.

A. Transverse and longitudinal beam dynamics modeling

The design for this tapered waveguide has been purposefully optimized to operate with a known electron source that will inject bunches into the waveguide. This electron source is a commercially available 100 keV , dc photoelectron gun [42], which our simulations show to be capable of delivering high-quality, low-energy spread bunches with durations on the order of a single picosecond [51]. This means that space charge plays a salient role in the bunch dynamics from the gun to the THz structure.

For our process of analyzing the dynamics of the interaction and assessing beam quality preservation, realistic electron bunches are needed to import into the CST PIC simulation and to compute dynamics of the THz-electron interaction. To achieve this, the electron gun is modeled using GPT. Bunches are created with an emittance and energy spread defined by the laser and the cathode. The gun features an LaB_6 photocathode, onto which ultraviolet (UV) pulses are directed. The UV pulses have a short duration, being produced via second-harmonic generation using a 30 fs laser system. This and other factors such as the low work function (2.5 eV) of the cathode, and the angle at which the UV pulse impinges, impact the initial bunch shaping. Immediately following the free-electron production, the bunch propagates in the blowout regime where space-charge broadening plays a dominating role. Electrons are accelerated to 100 keV over a dc voltage and can be generated with controllable charge. The accelerating, deflecting, and focusing fields in the gun are modeled explicitly, and the electron bunches are propagated to the waveguide entrance using a fifth order Runge-Kutta method to solve the particle evolution through the gun stages, and the drift section up to the waveguide. For modeling the bunch dynamics, the core elements of the gun (and therefore the GPT model) consist of the free-electron production, bunch shaping and acceleration by two anodes, and a solenoid which rotates and focuses the beam transversely into the DLW entrance. Upon reaching the THz structure, these realistic 100 keV bunches had a typical FWHM duration of $< 2 \text{ ps}$, an FWHM width of $80 \mu\text{m}$, and an energy spread of 0.05 keV , with some small variation to these parameters depending on the bunch charge. For this study, we have focused on studying the acceleration of relatively low $< 1 \text{ fC}$ charges, as this charge level allows the electron gun to

produce bunches of short duration without additional compression. In principle, however, there is nothing to prevent scaling up the charge accelerated by our tapered waveguides to an amount comparable with dc- and rf-driven electron sources if the bunches are compressed before acceleration. When modeling the THz-electron interaction using CST, a custom particle interface was used to import these realistic bunches from GPT.

B. Complete electron bunch dynamics for the 12 μJ , 25 mm structure

The LSM₁₁ mode utilized to give an on-axis accelerating field, also features significant transverse electric fields, particularly in the vertical, y direction. Field profiles for the vertical electric field can be seen in Fig. 4. The E_y field is 90° out of phase with the accelerating field so has zero field on crest and provides a focusing force and a defocusing force either side of the crest of the THz pulse. The focusing and defocusing forces originate from both quadrupolar and octopolar components of the LSM₁₁ mode [21] and exist in regions behind crest and ahead of the crest, respectively. The magnitude of these transverse forces increases approximately linearly as particles slip off-crest.

For the captured bunch that accelerates in approximate synchronism with the THz phase, significant transverse momentum can be imparted over the interaction duration. In our design, the captured bunch catches up with the on-crest phase in the initial stages, experiencing a defocusing force that decreases as it moves toward the crest. The positive off-crest phase of these particles throughout the central region of the DLW (≈ 5 to ≈ 20 mm) provides vertical focusing to the beam, restricting the emittance growth, before it slips back to a defocusing, negative off-crest phase in the final 5 mm. This causes the trajectory of the captured bunch to behave differently from other non-captured particles, meriting the independent analysis of its emittance growth and other properties.

Figure 10 shows energy spectra for two bunches after being accelerated through the structure with 12 μJ of injected power. A large energy peak at 162 keV can be seen in Fig. 10(a) where the 0.055 fC captured bunch is formed from the input 0.5 fC, 1.85 ps (FWHM) electron-gun bunch. Defining the capture rate as the charge contained in the accelerated peak as a proportion of the incoming charge, we find 11% for the electron gun bunch. Most particles do not receive significant acceleration due to not entering the waveguide in the initial capture region of the THz phase required to become synchronous and hence see an oscillation in the accelerating field along the length. Although the overall energy spread and acceleration percentage here are not directly competitive with that of dc or rf sources, we find a significant improvement when compressed bunches are injected. Using for example, a 185 fs input bunch which is identical but given a 10 \times compression longitudinally and a 2 \times compression vertically, the capture rate increases to 94%,

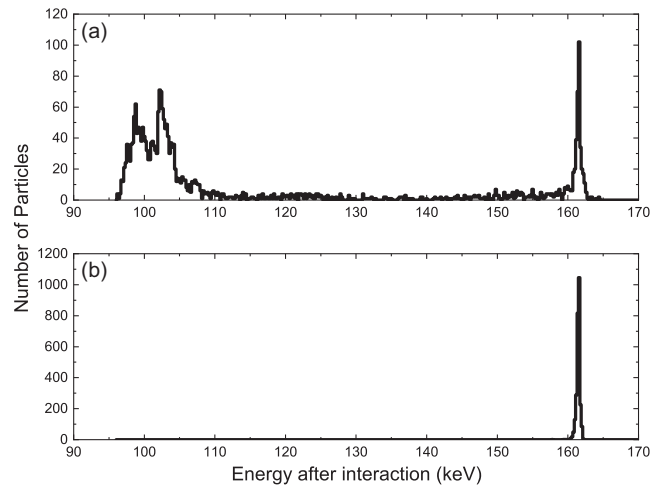


FIG. 10. Energy distribution of the whole bunch at the waveguide exit, with a realistic 100 keV 0.5 fC bunch tracked using GPT (a) and an idealized input bunch with 10% of the longitudinal size and 50% of the vertical size (b).

with all exiting particles being accelerated by > 40 keV. As shown in Fig. 10(b), this produces a clear single spike in the energy spectrum with a spread of 0.74 keV (FWHM), which is comparable with the energy spread of the dc-injected bunch. This makes the structure in question ideal for inclusion in a future compact THz beamline. Such a beamline could provide the compression and focusing suggested above by including a THz-driven compression stage, operating at the crossover phase, and a permanent magnet solenoid to provide additional transverse focusing into the accelerating structure.

Figure 11 shows the emittance growth for the captured bunch from a 0.3 fC bunch from the electron gun. The normalized vertical emittance of the captured bunch increases from 0.0226 mm mrad at the waveguide entrance to 0.549 mm mrad at the structure exit. This is driven primarily by strong quadrupolar and octopolar components of the transverse electric field. A small initial increase in emittance can be seen in the first roughly 7 mm of propagation due to the captured bunch primarily traveling in a defocusing phase of the E_y field. Simultaneously, space-charge forces cause the bunch to expand via Coulomb repulsion. These factors increase the vertical position and momentum spread that contribute to the emittance growth. For this initial stage of the interaction, the captured bunch propagates from 90° behind the accelerating crest and is catching up with the peak longitudinal field, meaning that the initial defocusing E_y field is strong at injection and decreases as the captured bunch moves toward an on-crest phase where the E_y field amplitude reaches zero. A sharp turn around in $\langle \beta_y^2 \rangle$ can be seen in Fig. 11(d) at 4 mm, where the captured bunch overshoots the crest and moves into the focusing E_y field. This deflects vertically off-center particles back toward an on-axis position. The effect of this vertical focusing then

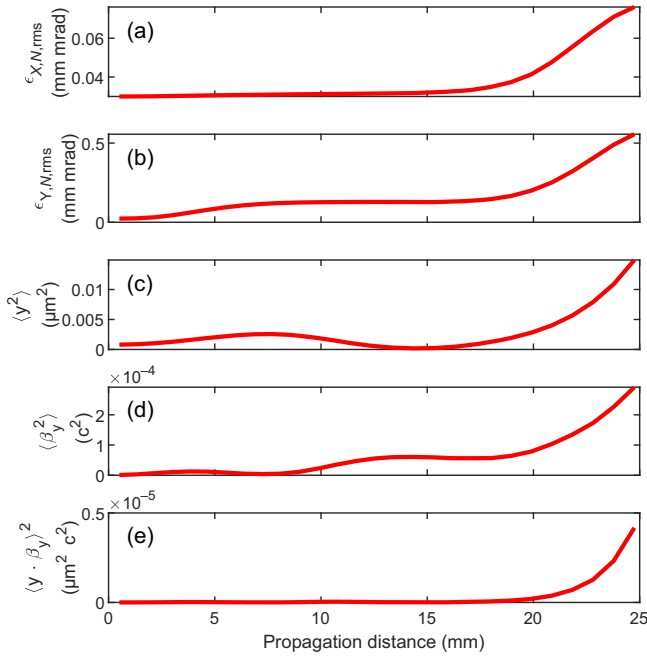


FIG. 11. Emittance growth for the captured bunch of a 0.3 fC bunch injected by a commercially available electron gun. (a) Normalized horizontal rms emittance, (b) normalized vertical rms emittance, (c) squared-mean vertical size, (d) squared-mean vertical momentum, and (e) correlation squared between vertical position and momentum.

carries through to give a similar turning point in the beam size [Fig. 11(c)], and these dynamics limit the vertical emittance growth in this region.

During propagation through the central portion of the waveguide, the captured bunch travels behind the crest of the accelerating field, corresponding to the vertically focusing region. The E_y field causes the captured bunch to pass through a focus at 15 mm as can be seen in Fig. 11(c), and the trajectories shown in Fig. 12(b), where the vertical size reduces to an amount smaller than that of the incoming beam. There is some overfocusing where the beam diverges again following the focus. Although the captured bunch is still propagating in the focusing region of the E_y field here, because it is now $< 30^\circ$ off-crest between 15 and 20 mm, the focusing strength is lower. This is also reflected in the way the squared vertical momentum spread $\langle \beta_y^2 \rangle$ stabilizes in this region [Fig. 11(d)].

In the final 5 mm of propagation, the captured bunch begins to diverge vertically again, increasing in both vertical position and momentum spread. This is primarily attributed to the captured bunch traveling in the defocusing phase of the E_y field in this region, where particles reach large amplitudes and are defocused by nonlinear fields. The strength of the E_y field experienced by these particles increases as they continue to move ahead of the E_z crest in this final stretch of the DLW. Various factors here serve to limit the emittance growth caused by the defocusing field,

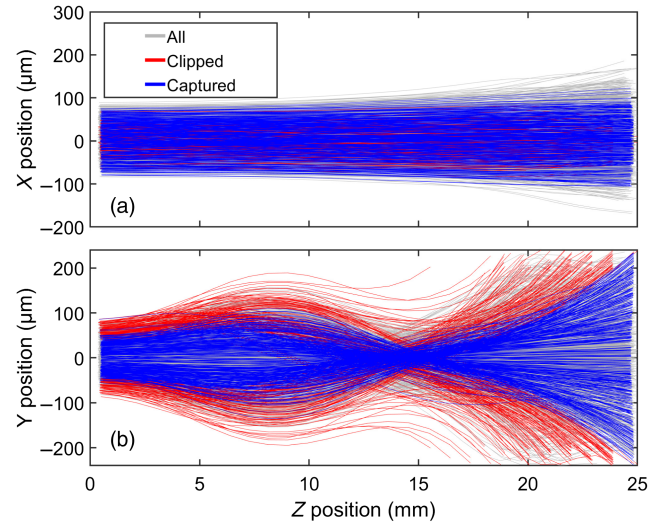


FIG. 12. Particle trajectories for a realistic 0.3 fC bunch from a commercially available electron gun propagating through the DLW. Trajectories for electrons which are lost due to being deflected into the dielectrics are highlighted in red, and electron trajectories for the particles in the captured bunch are highlighted in blue. The subplots show the (a) horizontal trajectories and (b) vertical trajectories.

including the increased beam rigidity following the > 50 keV of energy gain, pulse walk off from the captured bunch overtaking the THz pulse envelope, an increasing correlation between vertical position and momentum [Fig. 11(e)], and the loss of high $|y|$ and $|\beta_y|$ particles being deflected into the dielectric slabs. Because these clipped particles are those which have the most extreme vertical positions and momenta, eliminating these particles from the beam gives a collimationlike process which reduces the overall vertical spread and momentum growth. As observed in another study on cylindrical structures [39], this loss of particles with large vertical momenta was seen to lead to some decrease in the vertical emittance for the whole bunch.

The particle trajectories shown in Fig. 12 can be helpful in understanding how the emittance evolves during the acceleration. The effect of the E_y field can be seen in Fig. 12(b), and comparison with the off-crest phase of the captured bunch shown in Fig. 9 reveals a close alignment between the off-crest phase throughout the propagation, and the rate of focusing or defocusing in the trajectories. In the vertical trajectories, the regions of defocusing phase are from injection to 4 mm and from 20 mm to the exit. The region where the captured bunch occupies the focusing phase of the E_y field lies between 4 and 20 mm. The sign of the off-crest phase of the captured bunch can be interpreted as the direction of curvature of the blue paths (toward or away from center). The physical length of the whole bunch is evident in the vertical trajectories of Fig. 12; this is most obvious between 10 and 20 mm where the captured bunch

(blue) is being focused, whereas some of the clipped particles (red) that occupy different longitudinal positions of the bunch are being defocused. In rectangular DLWs, the transverse electric fields parallel to the plane of the dielectric slabs are lower than those that are orthogonal to the dielectric plane, which is why the horizontal trajectories in Fig. 12(a) show fewer features and no particles collide with the side walls or exceed the boundaries of the dielectric width in x . If any particles did exceed that x coordinate in a different design, they would experience lower field and fail to be captured into the accelerated bunch.

Transverse dependence to the accelerating field across the bunch is a general feature of structures with high operating frequencies, whether rectangular or cylindrical in geometry. Variation in the accelerating field vertically, indicated by the solid green line in Fig. 4, has some impact on the final phase space of the captured bunch in our structure. Particles exiting with small $|y|$ values were found to have a lower average energy than those closer to the dielectrics where the E_z field is stronger. A further effect of E_z field profile is seen in Fig. 13, where this induced particle velocity difference causes a “fishtail” shape to form after some propagation.

Due to the presence of a strong electric field in the vertical plane, some particles can be given enough transverse momentum to collide with the dielectric slabs that line the top and bottom of the vacuum channel. This is undesirable for a number of reasons. First, PIC simulations using realistic GPT-generated electron bunches showed that a large proportion ($\approx 70\%$) of particles that are deposited in the dielectrics are initially accelerated to energies surpassing 145 keV, suppressing the capture rate. These are particles that begin accelerating in close synchronism with the THz phase but occupy defocusing phase of the E_y field for an extended duration. This causes them to receive a coherent build up of transverse momentum during their propagation. Second, as the deposited electrons cannot be conducted away in the dielectric slabs, there is a static charge build up over time (especially if running at high repetition rates). This will exert some Coulomb repulsion

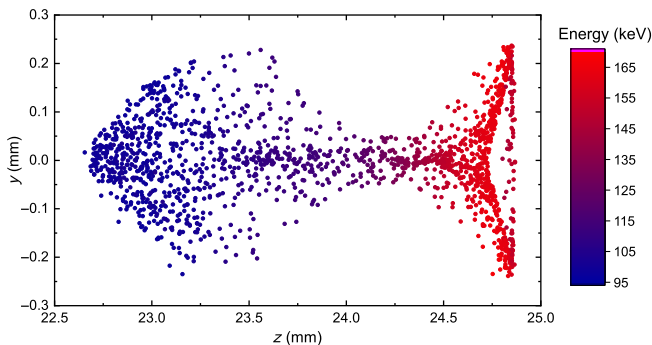


FIG. 13. Energy and y and z coordinates of particles immediately before the bunch leaves the DLW.

TABLE I. Properties of the captured bunch at the end of the propagation through the DLW. All spreads and lengths are given as FWHM. Data are shown for two cases using different starting bunches. The first is a realistic 0.5 fC electron gun bunch modeled in GPT, and the second uses the same bunch but is compressed by a factor of $10\times$ longitudinally, and a factor of $2\times$ vertically.

Property	Bunch from GPT	Compressed bunch
X spread (μm)	100	96
Y spread (μm)	239	177
Length (μm)	104	67
Duration (fs)	407	263
Charge (fC)	0.0667	0.4678
Mean energy (keV)	162	162
Energy spread (keV)	1.32	0.74
X emittance (mm mrad)	0.054	0.038
Y emittance (mm mrad)	0.371	0.093

on subsequent bunches and could disrupt the overall beam quality.

To minimize this effect, the length of the DLW section can be chosen to eliminate as much distance on the end as possible, without sacrificing energy gain. This is possible because, as shown in Fig. 14, the majority of the particle deposition occurs near the end of the structure. In an initial 30 mm long design, this region also offered negligible energy gain due to pulse walk off where the electron bunch had overtaken the low group-velocity THz pulse. Future experimental work will aim to quantify the impact of charging in this prototype design and determine a maximum safe repetition rate. Additionally, there is a potential to further reduce particle deposition with additional focusing magnets or an electrostatic lens near the waveguide entrance or by surrounding the DLW with a solenoid. Charging has also been partly mitigated in dielectric-loaded

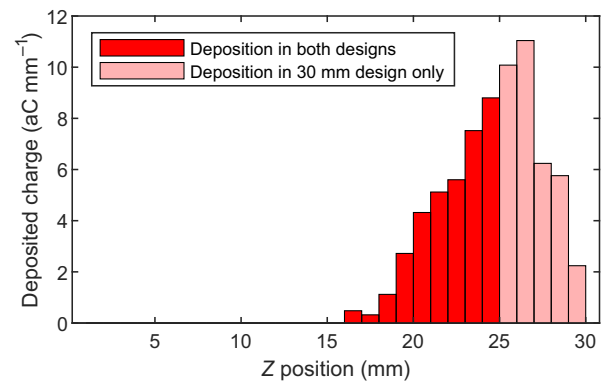


FIG. 14. Charge deposition rate vs longitudinal position for a realistic 0.3 fC bunch from a commercially available electron gun propagating through the tapered DLW. By shortening the length L of the DLW from 30 to 25 mm, some of the particle deposition (light red) was eliminated.

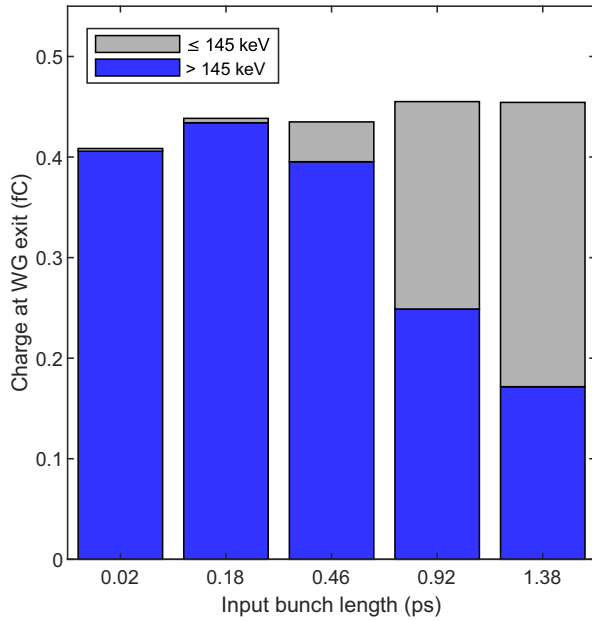


FIG. 15. Variation in the total transmitted charge and the accelerated charge for a 0.5 fC input bunch compressed by varying amounts. The proportion of charge that is accelerated increases for more compressed input bunches, while the total transmitted charge shows some decrease.

structures by applying a very thin (< 10 nm) coating of TiN on the dielectric surface [52].

The energy spread of the whole bunch is increased significantly for bunches with a duration longer than the capture region (see Fig. 8). The energy spread of the captured bunch however remains small as shown in Table I, as these particles accelerate synchronously with an accelerating bucket of the THz pulse throughout their interaction.

The energy gain a particle receives during the interaction is strongly dependent on its starting phase within the THz pulse. Particles not in the capture phase region at the beginning of the interaction do not receive enough velocity increase to remain synchronous for the rest of their propagation and therefore experience limited energy gain. The effect of this capture phase region can be seen in Fig. 15, where the amount of accelerated charge increases as the input bunch is compressed. For highly compressed input bunches, the proportion of electrons exiting the waveguide with significant energy gain (> 45 keV) is above 99%, however, a tail off in the total accelerated charge can be seen for very short input bunches. This is attributed to the entire input bunch now falling within the capture phase region, and from this point, the limiting factor on the accelerated charge becomes the particles being deposited in the dielectrics.

With the goal of maximizing the charge in the captured bunch, it becomes important not only to inject a short bunch solely occupying the capture phase region but also a bunch which is small vertically. Figure 16 shows how the capture

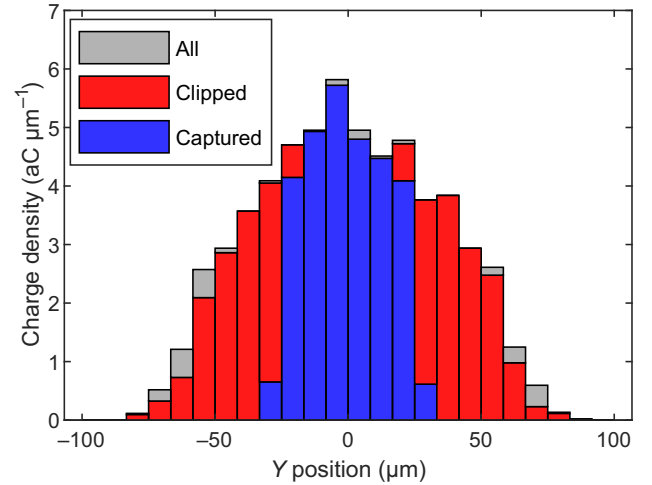


FIG. 16. Distribution of electron positions in y in a compressed 185 fs bunch upon entering the DLW. Particles that form the captured bunch begin close to on axis and are shown in blue. Particles that enter the DLW > 25 μm vertically off axis have a much higher chance to be deposited in the dielectrics downstream.

rate is close to 100% for particles entering the waveguide close to on axis vertically, while particles entering the waveguide off center in y are more likely to be deflected into the dielectrics. When using this accelerating waveguide in a beamline, it is therefore beneficial to include a simple focusing component, such as a permanent-magnet solenoid before the structure entrance, as this will greatly reduce charge loss and increase the capture rate.

IV. SCALING TO HIGHER ENERGIES

This paper has presented a design process with consideration of a commercial laser-driven THz source, taking a conservative estimate of available THz pulse energy. Good performance has been demonstrated close to the minimum suitable pulse energy and at a slightly higher value. In this section, we discuss what would be achievable when applying the same design process to a higher energy system.

Since the taper design must depend on the available gradient, simply injecting a higher energy pulse into the same structure would not improve performance. If the higher pulse energy was delivered over more cycles such that the field amplitude remained the same, a longer design with the same initial taper could work. However, in Fig. 8, it can be seen that as we taper to small widths, the group velocity falls off so the benefit of increasing pulse length will decrease as the pulse becomes longer. Instead, it is likely better to keep a similar pulse length but with higher amplitude.

Figure 17 shows the accelerating field needed to overcome larger velocity mismatches as given by Eq. (2). Note that this refers to the field in the structure, which depends on the dielectric thickness used. With a larger available

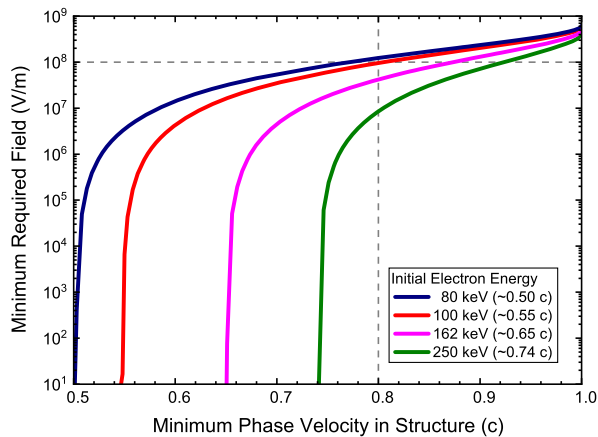


FIG. 17. Minimum accelerating field required to overcome the velocity mismatch in structures with different minimum phase velocities for a selection of example electron beam energies.

field amplitude, a larger velocity mismatch can be tolerated, thus allowing for a thinner dielectric which in turn improves on-axis field. This means that we can expect an above-linear improvement if we were to design a new structure for a significantly higher power laser-generated THz pulse than has been used here. The field needed for capture of a subrelativistic electron in a $v_p \approx c$ DLW would be very large, but the width-tapering method can be used in any rectangular DLW. The dashed reference lines in Fig. 17 show an example case of a 100 keV beam injected into a DLW with minimum phase velocity $0.8c$, which would require roughly 100 MV/m to overcome the mismatch after that the width tapering method up to $v_e \approx c$ could be applied. Figure 17 also illustrates the relevance of the tapering method with higher starting energies, with the 250 keV example still requiring some tapering to reach $v_e \approx c$ even when the accelerating field approaches 100 MV/m. With such high fields, transverse forces may present an issue, but as discussed in Sec. III B, this could be addressed with additional components for beam focusing and bunch compression.

Other than increasing THz energy, another way to reach relativistic energies is with a multistage approach wherein the output bunch from one accelerating structure is refocused to become the input bunch in another structure. Optimized THz-acceleration structures create electron bunches with very short duration and low-energy spread electron bunches. These two properties enhance capture as presented in Table I, thus making multistage acceleration systems a competitive option compared with higher energy dc sources. The challenging trade-off of requiring low on-axis field to match low phase velocities is most pronounced in the subrelativistic regime. Figure 17 includes the result for the final energy, 162 keV, of our low-energy design. As illustrated in Fig. 2, the modeled acceleration is much higher when using a thinner dielectric. Therefore, assuming the same pulse energy, a second stage would allow both a

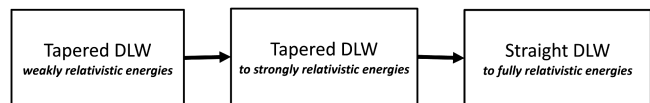


FIG. 18. A possible scheme for achieving fully relativistic energies by a multistage approach. Each stage would provide higher energy gain than the previous one, and the number of stages depends on the available THz pulse energy.

higher gradient and a larger velocity mismatch. It is hence reasonable to expect to reach fully relativistic energies with three or more structures as in Fig. 18. The number of stages needed and how much energy each stage can achieve would depend on the pulse energy available, but in any case, each stage after the first would be less challenging with respect to the velocity mismatch issue. Additionally, the change in velocity with increasing energy gets smaller as particles approach more highly relativistic energies, so the range of energies that can be covered with a similar amount of tapering increases each stage. As an example, we consider a rectangular DLW with a 250 μm fused silica lining. With the same operating frequency and starting widths ($w = w_d = 2.4$ mm) as our presented design, the phase velocity in this example DLW would be synchronous with 194 keV electrons and at the narrowest widths used ($w = 0.8$ mm, $w_d = 0.6$ mm), it would be synchronous with 1 MeV electrons, though pulse walk off means a single structure cannot cover that full range without a large increase in pulse duration and/or amplitude. When excited with the same 12 μJ 8-cycle pulse, the electric field on axis in an example 250 μm lined structure was over double that of the 380 μm lined structure. With a simple calculation to roughly estimate the interaction length, we can predict somewhere around 20 mm of interaction in each stage. We make a simplified estimate based on the on-crest field in a 2.4 mm wide structure at each energy level since this width is around that which gives the minimum synchronous energy in each case. The off-crest regions of interaction and the fact that the accelerating field increases significantly as the structure is tapered are not accounted for, but it is a suitable approximation to inform future design. Combining the estimations for gradient and interaction length, we can also make a rough estimate of the taper range of subsequent stages. A second stage with another 12 μJ pulse can be expected to increase our 162 keV output bunch to around 280 keV with a 250 μm silica layer tapering from $w = w_d = 2.4$ mm to $w = 1.4$ mm, $w_d = 0.8$ mm. A third stage with a 220 μm silica layer tapering from $w = w_d = 1.6$ mm to $w = 1.2$ mm, $w_d = 0.8$ mm would have higher gradient again over a similar interaction length and bring the bunch to around 450 keV. With this low-energy 12 μJ pulse, we therefore anticipate around six stages to reach 1 MeV. With a higher pulse energy, such as our 22.5 μJ example, fewer stages would be required. There also remains the possibility to study novel

techniques, such as phase shifters [38] or high- v_g regions to extend the interaction length, which may also reduce the number of structures needed.

Unlike cylindrical structures where the transverse forces are radial in nature, transverse effects in dielectric-slab lined rectangular waveguides are more sensitive in the y direction than the x direction, so aligning consecutive stages at 90° rotation relative to each other could further improve performance of a multistage design. This concept is discussed in [21] where an x - z -aligned DLW was followed by a y - z -aligned DLW, resulting in significant improvement in the emittance and energy spread after acceleration. The very low-energy spread of the output bunch is also expected to lower the complexity of a multistage approach. Depending on the pulse energy available, either high-gradient single stage or modest-gradient multistage approaches are viable. A combination of both these ideas may also offer good performance, such as raising the electron energy to, say, 200 keV in a low-energy structure, then injecting that bunch into a high-gradient system.

V. CONCLUSIONS

A design process for rectangular width-tapered dielectric-lined waveguides has been presented. Through particle-in-cell simulations, this type of structure was shown to provide an effective method for the acceleration of a subrelativistic 100 keV electron beam. The advantage of using narrowband THz pulses to prolong the interaction length and increase the electron energy gain has been previously shown; however, this remains a significant challenge in the subrelativistic regime where particle velocity depends strongly on energy. To overcome this challenge, a waveguide design methodology has been presented which uses hybrid width tapering to increase the THz phase velocity along the direction of propagation. The design process incorporated consideration of the manufacturing limitations on the dielectric lining, which limits how precisely the particle and phase velocities can be matched. It has been shown that despite this limitation, an effective taper profile still exists wherein the electron bunch can be kept in an accelerating phase for the full interaction length without exact matching. In fact, this mismatch of velocities proves necessary for low-pulse-energy designs, since electrons are injected below the lowest available phase velocity and overshoot the crest with the available gradient. We have shown that by then allowing phase velocity to increase more slowly than electron velocity, the bunch can be returned to crest and kept close to it until pulse walk off occurs.

The design process for a width-tapered DLW was described in detail, and the complete transverse and longitudinal electron beam dynamics of the interaction were explored. While the design was optimized for use with a commercially available electron gun, simulation results also showed the potential for capture rates above 90% using

a focused source of compressed electron bunches. In-parallel beam dynamic simulations enhanced the design process, and we were able to simulate acceleration of subrelativistic electron beams by an amount greater than previously demonstrated in THz-driven waveguides. Two designs were developed by means of the presented design process: one using a 22.5 μ J THz pulse and providing a THz-induced energy gain of 105 keV, and bunches with a 1% energy spread and FWHM duration of 343 fs, and a second using a 12 μ J THz pulse and providing an energy gain of 62 keV. The latter represents the acceleration achievable with close to the minimum on-axis field that allows capture in this DLW.

Discussion of scaling to higher energies using higher pulse energies or using a multistage approach has been presented. The outgoing bunch from the presented accelerating structure has a low-energy spread and short duration, suitable to be used as the input bunch for further acceleration in a second structure designed by the same methodology. The waveguide properties presented in this paper show that we can expect greater performance from subsequent stages. Therefore, a sequence of several tapered DLWs, each delivering more gain than the previous, could feasibly provide an initially subrelativistic beam with an energy increase to the MeV-level and ultrashort bunch lengths, making such a linac suitable for use as an injector for a higher energy machine, for medical and security applications, or for ultrafast electron diffraction imaging.

ACKNOWLEDGMENTS

We gratefully acknowledge P. Huggard of Rutherford Appleton Laboratory (RAL) for advice on the manufacturing tolerances, which helped ensure that the structure was designed subject to realistic machining limitations. This work was supported by the United Kingdom Science and Technology Facilities Council (Grant No. ST/V001612/1).

-
- [1] K. Nallappan, H. Guerboukha, Y. Cao, G. Xu, C. Nerguizian, D. Mittleman, and M. Skorobogatiy, *Terahertz Waveguides for Next Generation Communication Network* (CRC Press, Boca Raton, FL, 2021), pp. 379–410, [10.1201/9781003001140](https://doi.org/10.1201/9781003001140).
 - [2] J. Dong, A. Tomasino, G. Balistreri, P. You, A. Vorobiov, É. Charette, B. Le Drogoff, M. Chaker, A. Yurtsever, S. Stivala, M. A. Vincenti, C. D. Angelis, D. Kip, J. Azaña, and R. Morandotti, Versatile metal-wire waveguides for broadband terahertz signal processing and multiplexing, *Nat. Commun.* **13**, 741 (2022).
 - [3] Y. Cao, K. Nallappan, G. Xu, and M. Skorobogatiy, Add drop multiplexers for terahertz communications using two-wire waveguide-based plasmonic circuits, *Nat. Commun.* **13**, 4090 (2022).

- [4] W. Gao, X. Yu, M. Fujita, T. Nagatsuma, C. Fumeaux, and W. Withayachumnankul, Effective-medium-cladded dielectric waveguides for terahertz waves, *Opt. Express* **27**, 38721 (2019).
- [5] T. Ma, K. Nallapan, H. Guerboukha, and M. Skorobogatiy, Analog signal processing in the terahertz communication links using waveguide bragg gratings: Example of dispersion compensation, *Opt. Express* **25**, 11009 (2017).
- [6] O. Smolyanskaya *et al.*, Terahertz biophotonics as a tool for studies of dielectric and spectral properties of biological tissues and liquids, *Prog. Quantum Electron.* **62**, 1 (2018).
- [7] M. Walther, B. M. Fischer, A. Ortner, A. Bitzer, A. Thoman, and H. Helm, Chemical sensing and imaging with pulsed terahertz radiation, *Anal. Bioanal. Chem.* **397**, 1009 (2010).
- [8] X. Chen, H. Lindley-Hatcher, R. I. Stantchev, J. Wang, K. Li, A. Hernandez Serrano, Z. D. Taylor, E. Castro-Camus, and E. Pickwell-MacPherson, Terahertz (THz) biophotonics technology: Instrumentation, techniques, and biomedical applications, *Chem. Phys. Rev.* **3**, 011311 (2022).
- [9] B. You, J.-Y. Lu, C.-P. Yu, T.-A. Liu, and J.-L. Peng, Terahertz refractive index sensors using dielectric pipe waveguides, *Opt. Express* **20**, 5858 (2012).
- [10] G. Katyba, K. Zaytsev, I. Dolganova, N. Chernomyrdin, V. Ulitko, S. Rossolenko, I. Shikunova, and V. Kurlov, Sapphire waveguides and fibers for terahertz applications, *Prog. Cryst. Growth Charact. Mater.* **67**, 100523 (2021).
- [11] M. Awad and R. Cheville, Transmission terahertz waveguide-based imaging below the diffraction limit, *Appl. Phys. Lett.* **86**, 221107 (2005).
- [12] J. Li, K. Nallappan, H. Guerboukha, and M. Skorobogatiy, 3D printed hollow core terahertz Bragg waveguides with defect layers for surface sensing applications, *Opt. Express* **25**, 4126 (2017).
- [13] S. Atakaramians, V. Shahraam Afshar, T. M. Monro, and D. Abbott, Terahertz dielectric waveguides, *Adv. Opt. Photonics* **5**, 169 (2013).
- [14] J. A. Fülöp, S. Tzortzakos, and T. Kampfthaler, Laser-driven strong-field terahertz sources, *Adv. Opt. Mater.* **8**, 1900681 (2020).
- [15] E. A. Nanni, W. R. Huang, K.-H. Hong, K. Ravi, A. Fallahi, G. Moriena, R. J. D. Miller, and F. X. Kärtner, Terahertz-driven linear electron acceleration, *Nat. Commun.* **6**, 8486 (2015).
- [16] D. Zhang, A. Fallahi, M. Hemmer, X. Wu, M. Fakhari, Y. Hua, H. Çankaya, A.-L. Calendron, L. E. Zapata, N. H. Matlis, and F. X. Kärtner, Segmented terahertz electron accelerator and manipulator (STEAM), *Nat. Photonics* **12**, 336 (2018).
- [17] D. Zhang, M. Fakhari, H. Cankaya, A.-L. Calendron, N. H. Matlis, and F. X. Kärtner, Cascaded multicycle terahertz-driven ultrafast electron acceleration and manipulation, *Phys. Rev. X* **10**, 011067 (2020).
- [18] M. T. Hibberd, A. L. Healy, D. S. Lake, V. Georgiadis, E. J. H. Smith, O. J. Finlay, T. H. Pacey, J. K. Jones, Y. Saveliev, D. A. Walsh, E. W. Sneddon, R. B. Appleby, G. Burt, D. M. Graham, and S. P. Jamison, Acceleration of relativistic beams using laser-generated terahertz pulses, *Nat. Photonics* **14**, 755 (2020).
- [19] H. Tang, L. Zhao, P. Zhu, X. Zou, J. Qi, Y. Cheng, J. Qiu, X. Hu, W. Song, D. Xiang, and J. Zhang, Stable and scalable multistage terahertz-driven particle accelerator, *Phys. Rev. Lett.* **127**, 074801 (2021).
- [20] H. Xu, L. Yan, Y. Du, W. Huang, Q. Tian, R. Li, Y. Liang, S. Gu, J. Shi, and C. Tang, Cascaded high-gradient terahertz-driven acceleration of relativistic electron beams, *Nat. Photonics* **15**, 426 (2021).
- [21] Ö. Apsimon, G. Burt, R. B. Appleby, R. J. Apsimon, D. M. Graham, and S. P. Jamison, Six-dimensional phase space preservation in a terahertz-driven multistage dielectric-lined rectangular waveguide accelerator, *Phys. Rev. Accel. Beams* **24**, 121303 (2021).
- [22] H. Xu, R. Li, L. Yan, Y. Du, Q. Tian, W. Huang, and C. Tang, Towards a compact all optical terahertz-driven electron source at Tsinghua University, [arXiv:2206.02965](https://arxiv.org/abs/2206.02965).
- [23] X.-Q. Yu, Y.-S. Zeng, L.-W. Song, D.-Y. Kong, S.-B. Hao, J.-Y. Gui, X.-J. Yang, Y. Xu, X.-J. Wu, Y.-X. Leng, Y. Tian, and R.-X. Li, Megaelectronvolt electron acceleration driven by terahertz surface waves, *Nat. Photonics* **17**, 957 (2023).
- [24] A. L. Healy, G. Burt, and S. Jamison, Electron-terahertz interaction in dielectric-lined waveguide structures for electron manipulation, *Nucl. Instrum. Methods Phys. Res., Sect. A* **909**, 199 (2018).
- [25] F. Lemery, K. Floettmann, T. Vinatier, and R. W. Assman, A transverse deflection structure with dielectric-lined waveguides in the sub-THz regime, in *Proceedings of the 8th International Particle Accelerator Conference, IPAC-2017, Copenhagen, Denmark (JACoW, Geneva, Switzerland, 2017)*, p. 215, [10.18429/JACoW-IPAC2017-MOPAB052](https://doi.org/10.18429/JACoW-IPAC2017-MOPAB052).
- [26] L. Zhao, Z. Wang, H. Tang, R. Wang, Y. Cheng, C. Lu, T. Jiang, P. Zhu, L. Hu, W. Song, H. Wang, J. Qiu, R. Kostin, C. Jing, S. Antipov, P. Wang, J. Qi, Y. Cheng, D. Xiang, and J. Zhang, Terahertz oscilloscope for recording time information of ultrashort electron beams, *Phys. Rev. Lett.* **122**, 144801 (2019).
- [27] V. Georgiadis, A. L. Healy, M. T. Hibberd, G. Burt, S. P. Jamison, and D. M. Graham, Dispersion in dielectric-lined waveguides designed for terahertz-driven deflection of electron beams, *Appl. Phys. Lett.* **118**, 144102 (2021).
- [28] L. Zhao, H. Tang, C. Lu, T. Jiang, P. Zhu, L. Hu, W. Song, H. Wang, J. Qiu, C. Jing, S. Antipov, D. Xiang, and J. Zhang, Femtosecond relativistic electron beam with reduced timing jitter from THz driven beam compression, *Phys. Rev. Lett.* **124**, 054802 (2020).
- [29] L. J. Wong, A. Fallahi, and F. X. Kärtner, Compact electron acceleration and bunch compression in THz waveguides, *Opt. Express* **21**, 9792 (2013).
- [30] D. Zhang, A. Fallahi, M. Hemmer, H. Ye, M. Fakhari, Y. Hua, H. Cankaya, A.-L. Calendron, L. E. Zapata, N. H. Matlis, and F. X. Kärtner, Femtosecond phase control in high-field terahertz-driven ultrafast electron sources, *Optica* **6**, 872 (2019).
- [31] A. L. Healy, Energy modulation of electron bunches using a terahertz-driven dielectric-lined waveguide, doctoral thesis, Lancaster University, United Kingdom, 2020.
- [32] S. Antipov, C. Jing, M. Fedurin, W. Gai, A. Kanareykin, K. Kusche, P. Schoessow, V. Yakimenko, and A. Zholents,

- Experimental observation of energy modulation in electron beams passing through terahertz dielectric wakefield structures, *Phys. Rev. Lett.* **108**, 144801 (2012).
- [33] S. Antipov, M. Babzien, C. Jing, M. Fedurin, W. Gai, A. Kanareykin, K. Kusche, V. Yakimenko, and A. Zholents, Subpicosecond bunch train production for a tunable mJ level THz source, *Phys. Rev. Lett.* **111**, 134802 (2013).
- [34] Y. Xu, Y. Song, C.-Y. Tsai, J. Wang, Z. Liu, H. Qi, K. Fan, J. Yang, and O. I. Meshkov, Towards precise diagnosis time profile of ultrafast electron bunch trains using orthogonal terahertz streak camera, *Opt. Express* **31**, 19777 (2023).
- [35] E. A. Peralta, K. Soong, R. J. England, E. R. Colby, Z. Wu, B. Montazeri, C. McGuinness, J. McNeur, K. J. Leedle, D. Walz, E. B. Sozer, B. Cowan, B. Schwartz, G. Travish, and R. L. Byer, Demonstration of electron acceleration in a laser-driven dielectric microstructure, *Nature (London)* **503**, 91 (2013).
- [36] T. Chlouba, R. Shiloh, S. Kraus, L. Brückner, J. Litzel, and P. Hommelhoff, Coherent nanophotonic electron accelerator, *Nature (London)* **622**, 476 (2023).
- [37] P. Broaddus, T. Egenolf, D. S. Black, M. Murillo, C. Woodahl, Y. Miao, U. Niedermayer, R. L. Byer, K. J. Leedle, and O. Solgaard, Sub-relativistic alternating phase focusing dielectric laser accelerators, [arXiv:2310.02434](https://arxiv.org/abs/2310.02434).
- [38] D. Zhang, Y. Zeng, M. Fakhari, X. He, N. H. Matlis, and F. X. Kärtner, Long range terahertz driven electron acceleration using phase shifters, *Appl. Phys. Rev.* **9**, 031407 (2022).
- [39] F. Lemery, K. Floettmann, P. Piot, F. X. Kärtner, and R. Aßmann, Synchronous acceleration with tapered dielectric-lined waveguides, *Phys. Rev. Accel. Beams* **21**, 051302 (2018).
- [40] Z. Zhao, T. W. Hughes, S. Tan, H. Deng, N. Saprà, R. J. England, J. Vuckovic, J. S. Harris, R. L. Byer, and S. Fan, Design of a tapered slot waveguide dielectric laser accelerator for sub-relativistic electrons, *Opt. Express* **26**, 22801 (2018).
- [41] L. Xiao, W. Gai, and X. Sun, Field analysis of a dielectric-loaded rectangular waveguide accelerating structure, *Phys. Rev. E* **65**, 016505 (2001).
- [42] *EXGH-8121A/EGPS-8121A Manual*, Kimball Physics, Inc., 2017.
- [43] *Spitfire Ace Ultrafast Amplifier Manual*, Sprechta-Physics, 2011.
- [44] Simulia CST Studio Suite, Dassault Systemes, 2022.
- [45] S. Antipov, C. Jing, S. Baryshev, A. Kanareykin, S. Stoupin, W. Gai, A. Zholents, S. Baturin, M. Fedurin, and C. Swinson, Experimental test of semiconductor dechirper, in *Proceedings of the 6th International Particle Accelerator Conference, IPAC-2015, Richmond, VA (JACoW, Geneva, Switzerland, 2015)*, pp. 1932–1934, [10.18429/JACoW-IPAC2015-TUPMA043](https://doi.org/10.18429/JACoW-IPAC2015-TUPMA043).
- [46] Thomas P. Wangler, Longitudinal particle dynamics, in *RF Linear Accelerators* (John Wiley & Sons Ltd., Weinheim, Germany, 2008), Chap. 6, pp. 175–200, [10.1002/9783527623426](https://doi.org/10.1002/9783527623426).
- [47] S. V. Kutsaev, Electron bunchers for industrial RF linear accelerators: Theory and design guide, *Eur. Phys. J. Plus* **136**, 446 (2021).
- [48] C. D. Mosley, D. S. Lake, D. M. Graham, S. P. Jamison, R. B. Appleby, G. Burt, and M. T. Hibberd, Large-area periodically-poled lithium niobate wafer stacks optimized for high-energy narrowband terahertz generation, *Opt. Express* **31**, 4041 (2023).
- [49] W. K. H. Panofsky and W. A. Wenzel, Some considerations concerning the transverse deflection of charged particles in radio-frequency fields, *Rev. Sci. Instrum.* **27**, 967 (2004).
- [50] M. De Loos and S. Van der Geer, General particle tracer: A new 3D code for accelerator and beamline design, in *Proceedings of the 5th European Particle Accelerator Conference, EPAC-1996, Sitges, Barcelona, Spain (CERN, Geneva, Switzerland, 1996)*, Vol. 1241.
- [51] C. T. Shaw, O. Finlay, V. Georgiadis, M. T. Hibberd, D. S. Lake, R. Appleby, G. Burt, D. M. Graham, and S. P. Jamison, Terahertz diagnostic tool for sub-relativistic electron beams, in *Proceedings of the 47th International Conference on Infrared, Millimeter and Terahertz Waves, IRMMW-THz-2022, Delft, Netherlands (IEEE, New York, 2022)*, pp. 1–3, [10.1109/IRMMW-THz50927.2022.9895736](https://doi.org/10.1109/IRMMW-THz50927.2022.9895736).
- [52] C. Jing, W. Gai, J. Power, R. Konecny, S. Gold, W. Liu, and A. Kinkead, High-power RF tests on X-band dielectric-loaded accelerating structures, *IEEE Trans. Plasma Sci.* **33**, 1155 (2005).